

Optimal framework for quantitative magnetization transfer imaging of small structures

Marco Battiston¹, Francesco Grussu¹, Andrada Ianus^{2,3}, Torben Schneider⁴, Ferran Prados^{5,1}, James Fairney^{6,1}, Sebastien Ourselin⁵, Daniel C Alexander², Mara Cercignani⁷, Claudia A M Gandini Wheeler Kingshott^{1,8,9}, Rebecca S Samson¹

¹ *UCL Institute of Neurology, Queen Square MS Centre, University College London, London, United Kingdom*

² *Centre for Medical Image Computing, Department of Computer Science, University College London, London, United Kingdom*

³ *Champalimaud Neuroscience Programme, Champalimaud Centre for the Unknown, Lisbon, Portugal*

⁴ *Philips Healthcare, Guilford, Surrey, England*

⁵ *Translational Imaging Group, Centre for Medical Image Computing, Department of Medical Physics and Biomedical Engineering*

⁶ *UCL Department Medical Physics and Bioengineering, University College London, London, United Kingdom*

⁷ *CISC, Brighton & Sussex Medical School, Brighton, Sussex, United Kingdom*

⁸ *Department of Brain and Behavioural Sciences, University of Pavia, Pavia, Italy*

⁹ *Brain MRI 3T Mondino Research Center, C. Mondino National Neurological Institute, Pavia, Italy*

Synopsis:

Quantitative Magnetization Transfer (qMT) Imaging allows quantification of parameters describing the macromolecular component of tissues, potentially specific for myelin in the central nervous system. To date, applications of qMT in small structures (e.g. the spinal cord) have been hampered by prohibitively long acquisition. We present a framework for robust qMT examinations in small structures. It consists of: a dedicated MT-weighted sequence for small field-of-view imaging, explicit modelling of the non-steady state signal, and optimal definition of the sampling scheme. Superiority of the framework compared to a conventional qMT protocol is demonstrated in the healthy spinal cord and in the brainstem.

Purpose

Quantitative Magnetization Transfer (qMT) methods allow the conventionally inaccessible macromolecular component of tissues to be probed. In particular, qMT provides quantification of parameters such as the macromolecular fraction (BPF), macromolecular T_2 (T_2^B), free water T_2 (T_2^F), and free water to macromolecules exchange rate (k_{FB}), which have proven valuable in assessing myelin integrity in the central nervous system¹.

However, translation of qMT from the brain to small, yet key, structures, such as the spinal cord (SC), a primary location in demyelinating diseases, has not been fully implemented^{2,3}, as demands of high-resolution and adequate SNR result in prohibitive protocol lengths.

We propose a framework to enable robust assessment of qMT parameters in the SC within a clinically feasible scan time. An MT-weighted reduced Field-of-View echo-planar imaging (EPI) sequence is combined with a dedicated model for unbiased parameter estimation. The sampling scheme is optimized via Cramer-Rao-Lower-Bounds (CRLBs) minimization⁴. Reproducibility of qMT metrics is shown in the healthy SC, and the versatility of the framework for investigating other small structures is demonstrated in the brainstem, crucial for several neurodegenerative diseases and often characterized through MT imaging⁵.

Methods

Image acquisition is performed with ZOOM-EPI⁶. MT sensitization is achieved via an off-resonance pulse train preceding slice excitations. A numerical model based on the coupled Bloch equations⁷ is used for parameter estimation, to account for the non-steady-state nature of the acquisition. In addition to pulse amplitude (B_1) and offset frequency (Δ), effects of pulse duration (τ), inter-pulse gap (Δt) and number of pulses (N) are also modelled.

CRLB theory is used to derive configurations of ($B_1, \Delta, \tau, \Delta t, N$) that maximise precision of ($BPF, T_2^F, T_2^B, k_{FB}$), for a fixed number of data-points $K=14$ (+1 reference image), and under realistic SAR constraints. CRLBs are minimized using a self-organizing migratory algorithm (SOMA)⁸, to produce sets of optimal pairs (Δ, B_1). Remaining parameters ($\tau, \Delta t, N$) are selected by comparing a posteriori cost function values for optimisations at several combinations of ($\tau, \Delta t, N$). The cost function is given by the weighted mean of BPF, T_2^B and k_{FB} CRLBs.

The efficacy of optimization is tested using Monte Carlo simulations ($N=1000$ repetitions of Rician noise at $SNR=100, 50, 25, 18, 12$), comparing parameter estimate errors from the optimal protocol against a scheme based on standard steady-state qMT acquisition (i.e. uniform sampling)⁹.

Reproducibility indices (I) of qMT metrics, from a repeated acquisition (three times) on the same subject, are compared between optimal and uniform sampling. For a given parameter p , $I(p)$ is defined as $1 - \frac{1}{2} \frac{\max(p) - \min(p)}{\text{mean}(p)}$, where $I(p)=1$ means ideal reproducibility. Qualitative comparison of sampling schemes is performed in the brainstem to highlight the flexibility of the proposed framework.

In vivo imaging is performed on a 3T Philips Achieva system. The full protocol comprises 2 qMT acquisitions (optimal 21:27min, uniform 23:44min), and a shared Inversion-Recovery sequence (8

TIs, $TI_{\min}/\Delta t=150\text{ms}/350\text{ms}$) for T_1 estimation (15:06min); 12 axial slices are acquired at $0.75 \times 0.75 \times 5\text{mm}^3$ resolution in the SC, or at $0.9 \times 0.9 \times 3\text{mm}^3$ in the brainstem.

Results

Figure 1 shows optimised protocols producing low estimation errors and having little dependence on N by taking SAR and B_1 limits into account in the optimisation. For $N=25$, the best configuration for $(\tau, \Delta t)$ was found heuristically at $\tau/\Delta t=15\text{ms}/15\text{ms}$. Comparisons of optimal (Δ, B_1) sampling at $(\tau/\Delta t/N=15\text{ms}/15\text{ms}/25)$ and uniform sampling for simulations and in vivo are given in figure 2.

Monte-Carlo simulations demonstrate the superiority of optimal compared to uniform sampling, consistent at different SNR levels (fig.3).

In vivo, qMT parameters in the SC (fig.4) and brainstem (fig.5) show reduced variability when obtained from optimal sampling. The improvement over uniform sampling is particularly evident for k_{FB} . Reproducibility indices (uniform/optimal) in the SC are: $I(\text{BPF})=0.74/0.74$, $I(T_2^{\text{F}})=0.66/0.62$, $I(T_2^{\text{B}})=0.83/0.87$, $I(k_{\text{FB}})=0.58/0.82$.

Discussion and Conclusion

We combine explicit modelling of the non-steady-state MT signal and protocol optimization to simultaneously improve parameter estimates and shorten scan time compared to conventional sampling.

k_{FB} is the parameter that benefits the most from optimisation, given its large intrinsic variability as previously reported¹⁰. Reproducibility index did not show improvements in BPF, therefore further investigations are needed to clarify this aspect, including specific protocol optimisations targeting only BPF.

Our framework allows to choose pulse-train duty cycle and duration independently, which we exploit for shorter and more efficient protocols. Here, optimal configuration for $(\tau, \Delta t, N)$ was found empirically, which could lead to suboptimal protocols. The full set of sequence parameters will be optimized simultaneously in future analysis.

The proposed framework is versatile and can be used for any type of localized qMT examination. We have demonstrated its applicability to the brainstem, to delineate differences between the substantia nigra and the surrounding white matter, and provide new complementary information towards the characterization of this structure using MT¹¹.

Acknowledgements

The UK MS Society; NIHR BRC UCLH/UCL High Impact Initiative-BW.mn.BRC10269; Horizon2020-EU3.1 CDS-QUAMRI (ref: 634541); Project grants EPSRC EP/I027084/1 and ISRT IMG006; MRC(MR/J500422/1); Project grants EPSRC (EP/H046410/1, EP/J020990/1, EP/K005278) and MRC (MR/J01107X/1).

References

- [1] Sled J, Pike B. Quantitative imaging of magnetization transfer exchange and relaxation properties in vivo using MRI. *Magnetic resonance in medicine* 46.5(2001):923-931.
- [2] Smith S, Golay X, Fatemi A, et al. Quantitative magnetization transfer characteristics of the human cervical spinal cord in vivo: application to adrenomyeloneuropathy. *Magnetic resonance in medicine* 61.1(2009):22-27.
- [3] Smith A, Dortch R, Dethrage L, et al. Rapid, high-resolution quantitative magnetization transfer MRI of the human spinal cord. *NeuroImage* 95(2014):106-116.
- [4] Atkinson A, Donev A. *Optimum experimental design*. Oxford: Oxford University Press (1992).
- [5] Tambasco N, Nigro P, Romoli M, et al. Magnetization transfer MRI in dementia disorders, Huntington's disease and parkinsonism. *Journal of the neurological sciences* 353.1(2015):1-8.
- [6] Wheeler-Kingshott C, Hickman S, Parker G, et al. Investigating cervical spinal cord structure using axial diffusion tensor imaging. *Neuroimage* 16.1(2002):93-102.
- [7] Portnoy S, Stanisz G. Modeling pulsed magnetization transfer. *Magnetic resonance in medicine* 58.1(2007):144-155.
- [8] Alexander D. A general framework for experiment design in diffusion MRI and its application in measuring direct tissue-microstructure features. *Magnetic Resonance in Medicine* 60.2(2008):439-448.
- [9] Cercignani M, Symms M, Schmierer K, et al. Three-dimensional quantitative magnetisation transfer imaging of the human brain. *Neuroimage* 27.2(2005):436-441.
- [10] Cercignani Mara, Alexander D. Optimal acquisition schemes for in vivo quantitative magnetization transfer MRI. *Magnetic resonance in medicine* 56.4(2006):803-810.
- [11] Helms G, Draganski B, Frakowiak R, et al. Improved segmentation of deep brain grey matter structures using magnetization transfer (MT) parameter maps. *Neuroimage* 47.1(2009):194-198.

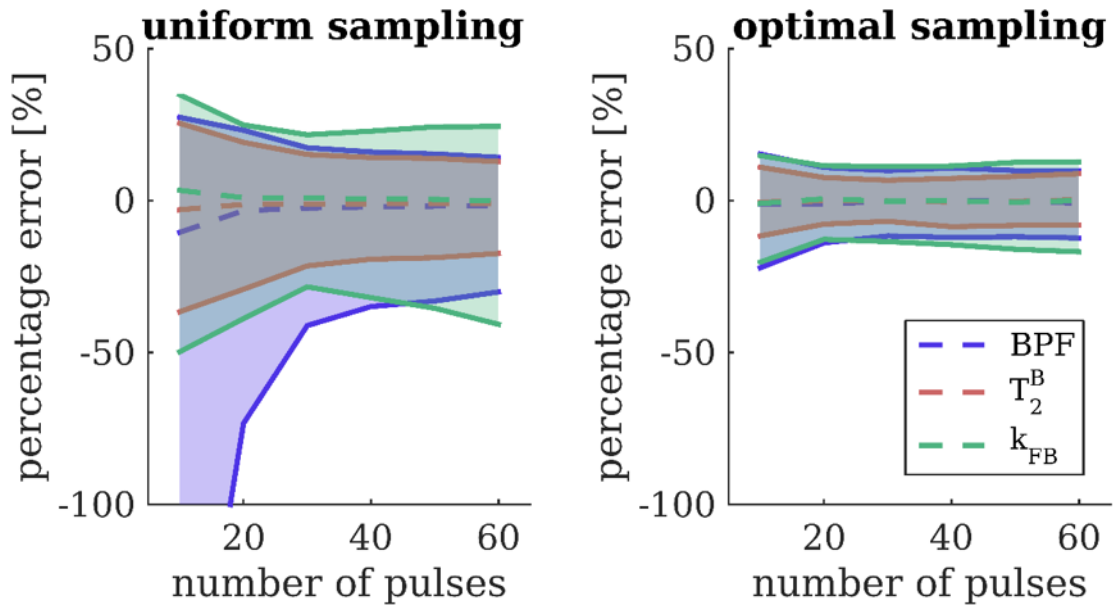


Figure 1: Heuristic search of optimal train length. Estimate error distributions for uniform samplings (left) and optimal samplings (right) protocols at varying length of pulse train, for $\tau/\Delta t=20\text{ms}/20\text{ms}$. Errors dependency on train length can be greatly reduced through protocol optimisation.

uniform sampling		optimal sampling	
flip angle	offset	flip angle	offset
[°]	[Hz]	[°]	[Hz]
601°	400	393°	1311
601°	768	1471°	3283
601°	1474	426°	1706
601°	2828	1471°	3420
601°	5429	383°	1031
601°	10420	1464°	1000
601°	20000	378°	1018
1100°	400	1470°	3348
1100°	768	385°	1029
1100°	1474	1471°	13985
1100°	2828	1466°	3250
1100°	5429	456°	2102
1100°	10420	1467°	3517
1100°	20000	1427°	13710

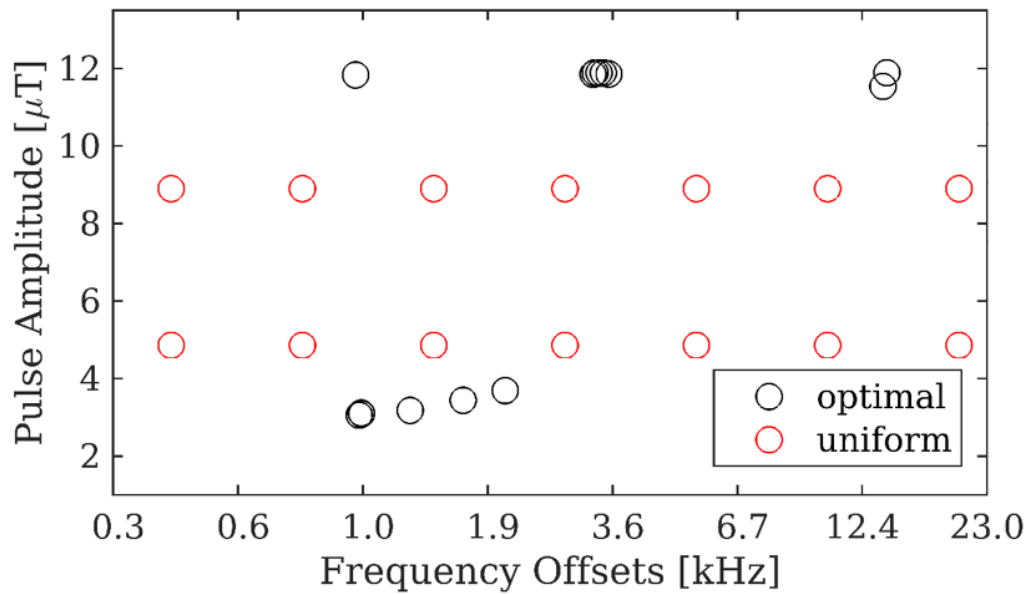


Figure 2. Sampled pairs (Δ, B_1) for uniform (left) and optimal (right) protocols, and diagram of sampling points in the plane (Δ, B_1) . For the uniform protocol, offset frequencies are logarithmically spaced between 400Hz and 20kHz, distributed among 2 different RF powers corresponding to 80% and 30% of the SAR limit. Other sequence parameters are: $\Delta t \setminus \tau = 15\text{ms} \setminus 15\text{ms}$ for both protocols. $N=25$ in optimal sampling, while $N=50$ in uniform sampling, in order to approach the steady-state condition.

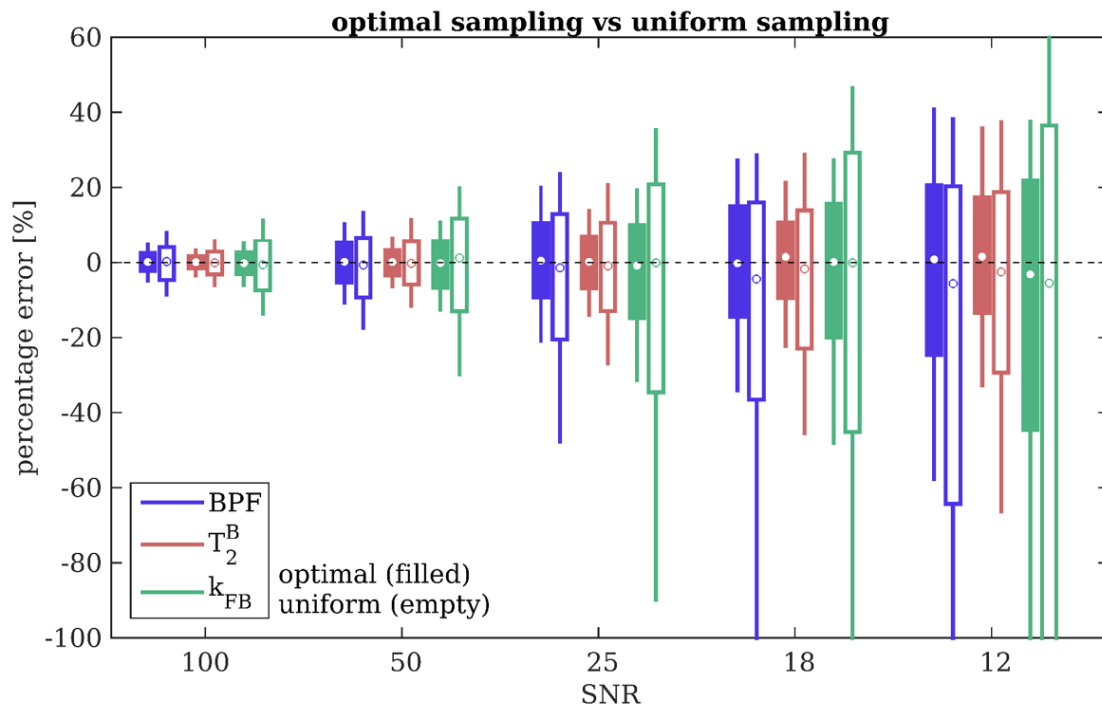


Figure 3: Distribution of estimate errors from Monte Carlo simulations performed at $N=1000$ realizations of Rician noise at different levels of $SNR=100,50,25,18,12$, for optimal sampling (filled boxplots) and uniform sampling (unfilled boxplots). The SNR regime for the in vivo experiments performed is expected to be between 18 and 25.

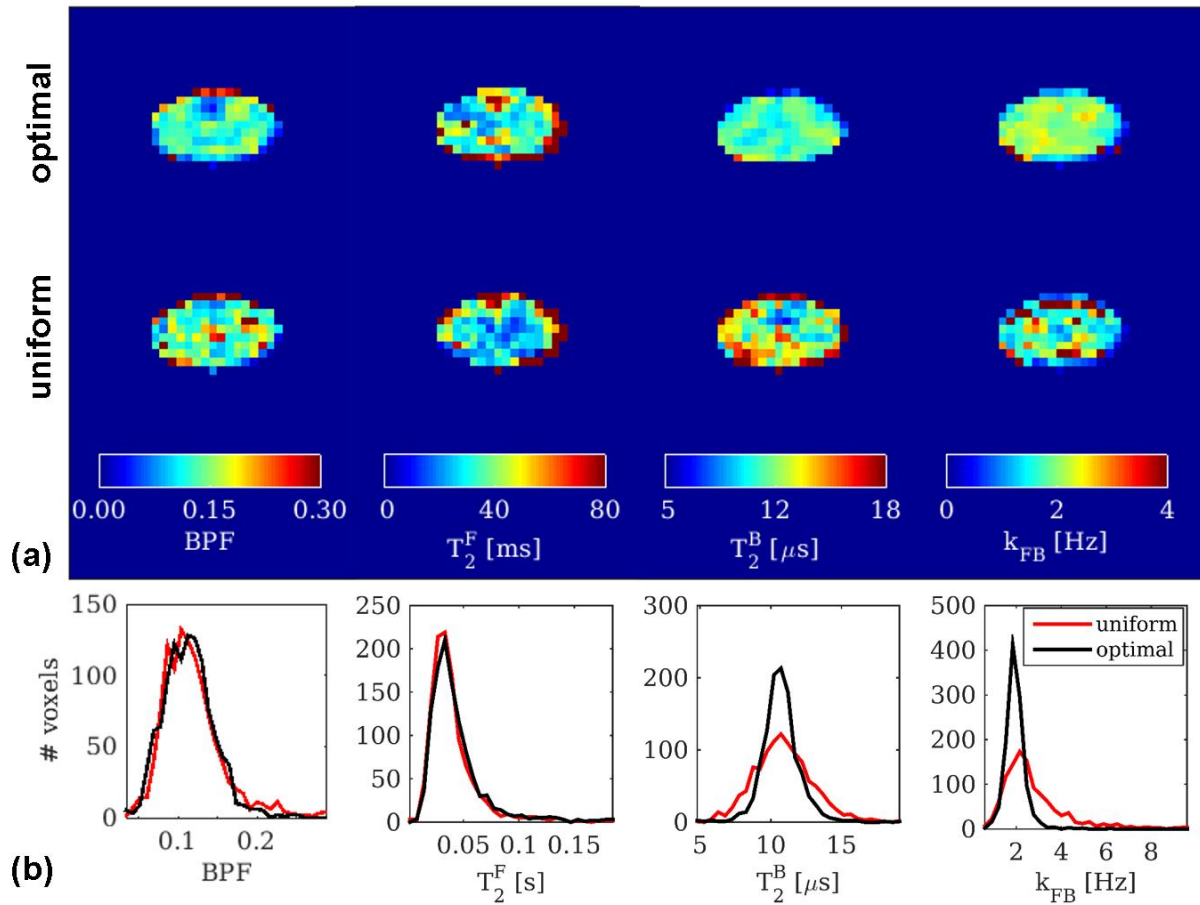


Figure 4a: comparison in an example slice of qMT parameter maps between optimal sampling (top row), and uniform sampling (bottom row). Figure 4b: Parameter distributions over the whole portion of the cord imaged (6cm centred at c2/c3 disc) for optimal (black trace) and uniform (red trace) protocols.

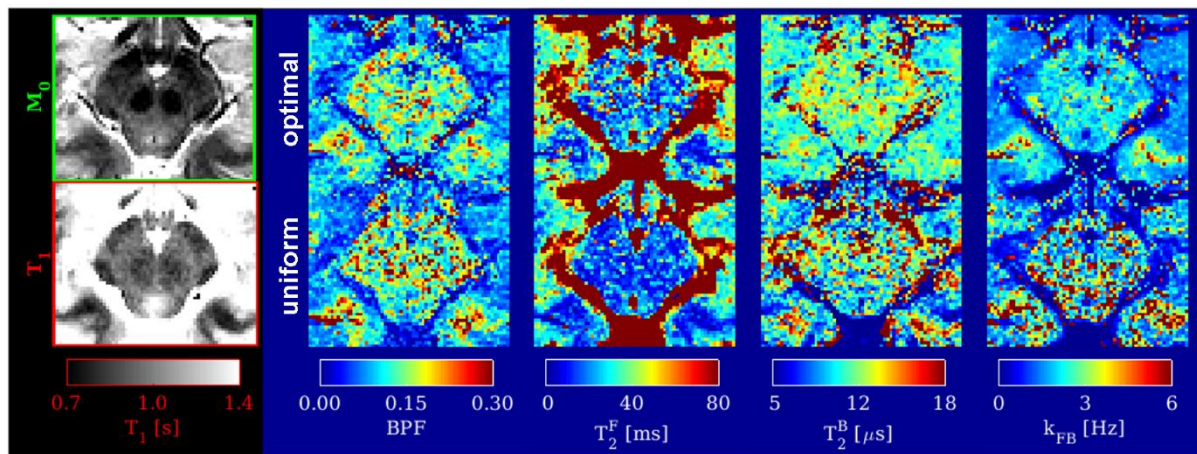


Figure 5: Comparison of qMT parametric maps in the brainstem, at the level of the substantia nigra, for optimal (top row) and uniform (bottom row) samplings. The effect of protocol optimisation is appreciable in parameters included in the optimisation (i.e. BPF, T_2^B and k_{FB}). In the first column quantitative maps obtained from IR experiment, i.e. equilibrium magnetization M_0 (top) and longitudinal relaxation time T_1 (bottom), shared among qMT protocols, are shown for the same example slice.